Electrochimica Acta 269 (2018) 172–179

Contents lists available at ScienceDirect

Electrochimica Acta

journal homepage: www.elsevier.com/locate/electacta

A novel, PbS:Hg quantum dot-sensitized, highly efficient solar cell structure with triple layered TiO_2 photoanode

M.A.K.L. Dissanayake [a, b, *], T. Jaseetharan [a, b], G.K.R. Senadeera [a, c], C.A. Thotawatthage [a, b]

[a] National Institute of Fundamental Studies, Kandy, Sri Lanka
[b] Postgraduate Institute of Science, University of Peradeniya, Peradeniya, Sri Lanka
[c] Department of Physics, The Open University of Sri Lanka, Nawala, Nugegoda, Sri Lanka

ARTICLE INFO

Article history:
Received 13 January 2018
Received in revised form
18 February 2018
Accepted 25 February 2018
Available online 2 March 2018

Keywords:
Quantum dot-sensitized solar cells
TiO_2 tri-layer photonanode
Electrochemical impedance spectroscopy
Multiple exciton generation
Quantum confinement effect

ABSTRACT

Hg-doped PbS quantum dot-sensitized solar cells (QDSSCs) were fabricated using successive ionic layer adsorption and reaction method with TiO_2 single layer, double layer and triple layer photoanode nanostructures. The triple layer TiO_2 photoanode was fabricated by using a TiO_2 nanofibre (NF) layer sandwiched between two TiO_2 nanoparticle (NP) layers in order to enhance light harvesting through effective light scattering process. The performance of this photoanode has been further enhanced by the surface charge control process and mild annealing treatment. TiO_2 triple layer nanostructure based QDSSC showed a significantly higher energy conversion efficiency of 4.72% under the simulated light of 100 mW cm^{-2} with AM 1.5 filter. The efficiency of the best solar cell made with a single layer of TiO_2 nanoparticles under the same conditions was 2.94%. The enhanced solar cell efficiency has been attributed to improved light harvesting by multiple light scattering in the tri-layer TiO_2 photoanode structure combined with efficient electron transport with less recombination as evidenced from electrochemical impedance spectroscopic measurements.

1. Introduction

Semiconductor quantum dots have been studied under various research areas such as solar cells, light emitting diodes, lasers, spectrometers and infrared detectors due to their size – dependent optoelectronic properties and low fabrication cost [1–6]. Quantum dot-sensitized solar cells (QDSSCs) are emerging as a promising third generation photovoltaic system for cost-efficient solar energy conversion applications compared to TiO_2 based dye-sensitized solar cells which generally use more expensive inorganic dyes. In a QDSSC, quantum dots act as light absorbing material which has high molar extinction coefficients, ability of multiple exciton generation and tunable energy gap due to the quantum confinement effect. Intensive research studies have been performed to fabricate different types of QDSSCs based on semiconductor quantum dots such as PbS, CdS, PbS/CdS, CdSe, PbSe, $CuInS_2$/CdS, CdS/CdSe, CdTe and Sb_2Se_3 [7–15]. To enhance the photovoltaic performance of QDSSCs, many studies have also been performed on photoanodes based on different semiconductor oxides such as ZnO, TiO_2 and SnO_2 and with different nanostructures such as nanopowders, nanotubes, nanofibres, nanohelixes etc. The energy conversion efficiency of dye-sensitized solar cells can generally be enhanced by increasing the light harvesting through the light scattering. For this purpose, semiconductor multilayer photoanode structures can be used. Recently, TiO_2 nanoparticle/TiO_2 nanofibre/TiO_2 nanoparticle triple layer photoanode based dye-sensitized solar cells with enhanced energy conversion efficiencies of 8.8% and 7.30% have been reported [16,17].

PbS is a narrow band gap p-type semiconductor with a large exciton Bohr radius of about 18 nm, a high absorption coefficient and an excellent photosensitivity in the near-infrared region. PbS quantum dots are used as photo sensitizers to extend the light harvesting region to near – infrared wavelengths in solar cell applications [18]. Recently, ZnO based PbI_2-capped PbS solid state QDSSC was reported with power conversion efficiency of 3.7% [19]. In another study, PbS QDSSC based on TiO_2 nanotube array has been fabricated with an efficiency of 3.41% [20]. There are several techniques that have been used for the fabrication of quantum dots on nanostructure of semiconductor oxides, such as chemical bath deposition (CBD) method and successive ionic layer adsorption and

* Corresponding author. National Institute of Fundamental Studies, Kandy, Sri Lanka.
E-mail address: makldis@yahoo.com (M.A.K.L. Dissanayake).

https://doi.org/10.1016/j.electacta.2018.02.140
0013-4686/

reaction (SILAR) method, spin assisted SILAR and electrostatic adsorption method. SILAR method is widely used and also the properties of the QDs can be easily controlled by varying the concentration of precursor solutions, number of dipping cycles, dipping duration, pH of the precursor solutions and SILAR temperature. In a related study of PbS-sensitized QDSSCs, the temperature of the precursor solution has been optimized to obtain a power conversion efficiency of 3.88% with a high photocurrent density of 30.1 mA cm^{-2} [21].

Power conversion efficiency of QDSSCs has been enhanced also by controlling the surface charge of TiO_2 nanostructure using a weak base such as triethanolamine [22]. Power conversion efficiency can be further enhanced by doping of the semiconductor. Hg - doped PbS, Mn-doped PbS and Mn-doped CdS QDSSCs have been reported with power conversion efficiencies of 2.49%, 4.25%, and 5.4% respectively [22–24]. In another study, the overall performance of the PbS QDSSCs has been enhanced by mild annealing of the photo electrode [25]. In order to enhance the power conversion efficiency of QDSSCs it is important to have a compatible electrolyte and a counter electrode. There are several studies that have been performed in order to find a suitable electrolyte for QDSSCs and polysulfide electrolyte has been widely recommended as a suitable electrolyte. In these studies, Cu_2S has been used as a counter electrode compatible with the polysulfide electrolyte [26,27].

In the present study, Hg-doped PbS quantum dots were deposited on different TiO_2 nanostructure layers using SILAR method and QDSSCs have been fabricated and characterized. A novel TiO_2 triple layer photoanode structure incorporating PbS:Hg Q-dots has been introduced to enhance the short circuit photocurrent density and the energy conversion efficiency through improved light harvesting. The performance of the solar cells has been further enhanced by mild annealing of PbS:Hg quantum dot – sensitized photoanode and surface charge control using triethanolamine (TEA). This is the first successful attempt to show that the enhancement of efficiency using the TiO_2 nanoparticle/nanofibre/nanoparticle tri-layer photoanode works equally well also for Q-dot sensitized solar cells.

2. Experimental

2.1. Materials

Fluorine-doped tin oxide (FTO) coated glass (8 Ω cm^{-2},Solarnoix), methanol (99.8%, Sigma-Aldrich), Titanium (iv) isopropoxide (97%, Fluka), propan-1-ol (99.9%, Fisher), glacial acetic acid (99%, Fisher), ethanol(96%, BDH), titanium dioxide P-90 powder (Evonik, Germany), Titanium dioxide P-25 powder (Degussa), poly ethylene glycol (99.8%, Sigma-Aldrich), triton X-100 (Sigma-Aldrich), Lead(ii) nitrate (99%, Sigma-Aldrich), mercury(ii) chloride (99.5%, Sigma-Aldrich), sodium sulfide hydrate (>60%, Sigma-Aldrich), triethanolamine (99%, Fluka), potassium chloride (99%, Sigma-Aldrich), Sulfur (99%, Daejng), hydrochloric acid (37%, Sigma-Aldrich) were used as received without further purification or treatment.

2.2. Preparation of TiO_2 triplelayer nanostructure

A pin hole free compact layer of TiO_2 was first deposited on precleaned FTO glass substrate by the following method. 1 ml of titanium (iv) isopropoxide, 1 ml of propan-1-ol, 1 ml of glacial acetic acid and 1 drop of con. HNO_3 were added to 8 ml of ethanol and the mixture was mixed well. This nanoparticle solution was then spin coated on FTO glass substrate at 3000 rpm for 1 min. Substrates were then sintered at 120 °C for 5 min. Again the same solution was spin coated at 3000 rpm for 1 min on the above TiO_2 layer and then sintered at 450 °C for 45 min.

The above substrate with compact layers was then covered with a paste prepared with P-90 TiO_2 as follows. 0.25 g of TiO_2 P-90 powder was ground well for 15 min with 1 ml of 0.1 M HNO_3. The paste was spin coated on the TiO_2 compact layer at 3000 rpm for 1 min and sintered at 450 °C for 45 min.

For the fabrication of the active TiO_2 nanofibre (NF) layer, 1.5 ml of titanium (iv) isopropoxide, 0.75 g of poly(vinylacetate) and 0.5 ml of glacial acetic acid were mixed in 9.5 ml of N,N-dimethyl foramide (DMF) and the mixture was subjected to magnetic stirring for 4 h. Then TiO_2 nanofibre layer was electrospun on the TiO_2 nanoparticle layer using an electrospinning system (NaBond Technologies, Hong Kong). Initially, the cylindrical drum collector was electrically grounded and the conducting glass plates (FTO/CL/P-90/P-25) with the TiO_2 nanoparticle layer were fixed on the surface of the drum collector. During electrospinning, the distance and voltage difference between the drum collector and the spinneret were kept at 6.5 cm and 15 kV respectively. Electrospinning was done for 20 min with the drum collector rotating at 270 rpm and a controlled rate of flow of 2 ml/h of the electrospinning solution. Electrodes with TiO_2 NP/NF double layer were sintered at 450 °C for 45 min. Finally, a TiO_2 P-25 layer was spin coated on the above TiO_2 nanofibre layer at 1000 rpm for 1 min and sintered at 450 °C for 45 min to obtain the TiO_2 NP/NF/NP tri-layer photoanode structure.

In order to compare the photovoltaic performance, three different types of TiO_2 nanostructure photoanodes with similar thickness of about 3.45 μm were fabricated as follows on FTO/CL/P-90 substrate.

(a) Single layer TiO_2 nanoparticle (NP)
(b) Double layer TiO_2 nanoparticle/TiO_2 nanofibre (NP/NF)
(c) Triple layer TiO_2 nanoparticle/TiO_2 nanofibre/TiO_2 nanoparticle (NP/NF/NP)

2.3. Deposition of Hg-doped PbS quantum dots

Mercury – doped lead sulfide (PbS:Hg) quantum dots were deposited on each layer of TiO_2 nano-porous structure by SILAR method. Here, de-ionized water was used as a solvent. Cationic precursor solution contained 0.1 M $Pb(NO_3)_2$, 6 mM $HgCl_2$ and 0.8 M triethanolamine (TEA) while anionic precursor solution contained 0.1 M Na_2S. Initially, TiO_2 electrode was dipped in the cationic precursor solution for 1 min followed by dipping in the anionic precursor solution for 1.5 min. The electrode was rinsed with de-ionized water and dried in between each dipping process. This two step dipping is known as one SILAR cycle. In this study, 6 SILAR cycles were used to deposit PbS:Hg QDs on each TiO_2 nanostructure as 6 cycles were found to give the best solar cell performance. Each type of PbS:Hg quantum dot – incorporated TiO_2 electrode was sintered at 120 °C for 10 min and allowed to cool. Finally, the electrode was immersed in an aqueous solution of 0.1 M Na_2S for 1 min and rinsed with de-ionized water.

2.4. Preparation of the polysulfide electrolyte

2 M Na_2S, 2 M S and 0.2 M KCl solutions were prepared by dissolving them in a mixture of water and methanol in the ratio of 3:7 (v/v). The mixture was subjected to magnetic stirring at room temperature until all the sulfur was dissolved.

2.5. Preparation of Cu_2S counter electrode

A cleaned brass plate was immersed in conc. HCl at 80 °C for 10 min. A scotch tape mask with appropriate area was applied on

the surface of the treated brass plate. Poly sulfide electrolyte was applied to the unmasked area which became black colour due to the formation of Cu_2S.This was used as the counter electrode of the QDSSCs.

2.6. Absorption measurements

To study the light harvesting performance of the photoanodes, optical absorption spectra of PbS:Hg quantum dot-loaded TiO_2 nanostructures with equal thickness were obtained using Shimadzu 2450 UV–VIS spectrophotometer in the wavelength interval from 350 nm to 1100 nm.

2.7. Cell assembly

In order to fabricate a quantum dot sensitized solar cell, an appropriate amount of poly sulfide electrolyte was applied on the unmasked area of the Cu_2S counter electrode. A TiO_2 photoanode plate was placed on the electrolyte so that the active sides of both electrodes were facing each other with the electrolyte in between them. The cell assembly was held together using steel clips.

2.8. Current -voltage characterization

To study the photovoltaic performance of the QDSSCs, current density-voltage ($J-V$) measurements of solar cells with each type of PbS:Hg incorporated TiO_2 photoanode were done under the illumination of 100 mW cm^{-2} with AM 1.5 spectral filter using a computer controlled multi-meter (Keithley 2000 model) coupled with potentiostat/galvanostat unit (HA-301). The active area of the QDSSC was 0.12 cm^2.

2.9. Electrochemical impedance spectra (EIS) measurements

Electrochemical impedance measurement is an important and essential measurement to characterize the electrochemical performance of each component and interfaces of solar cells [28]. Chemical capacitance, carrier transport resistance, recombination resistance and series resistance can be calculated by fitting the electrochemical impedance spectroscopy (EIS) data with an appropriate equivalent circuit of the QDSSC. Electron lifetime, electron diffusion length and effective diffusion coefficient can also be determined from these measurements. Impedance spectra of

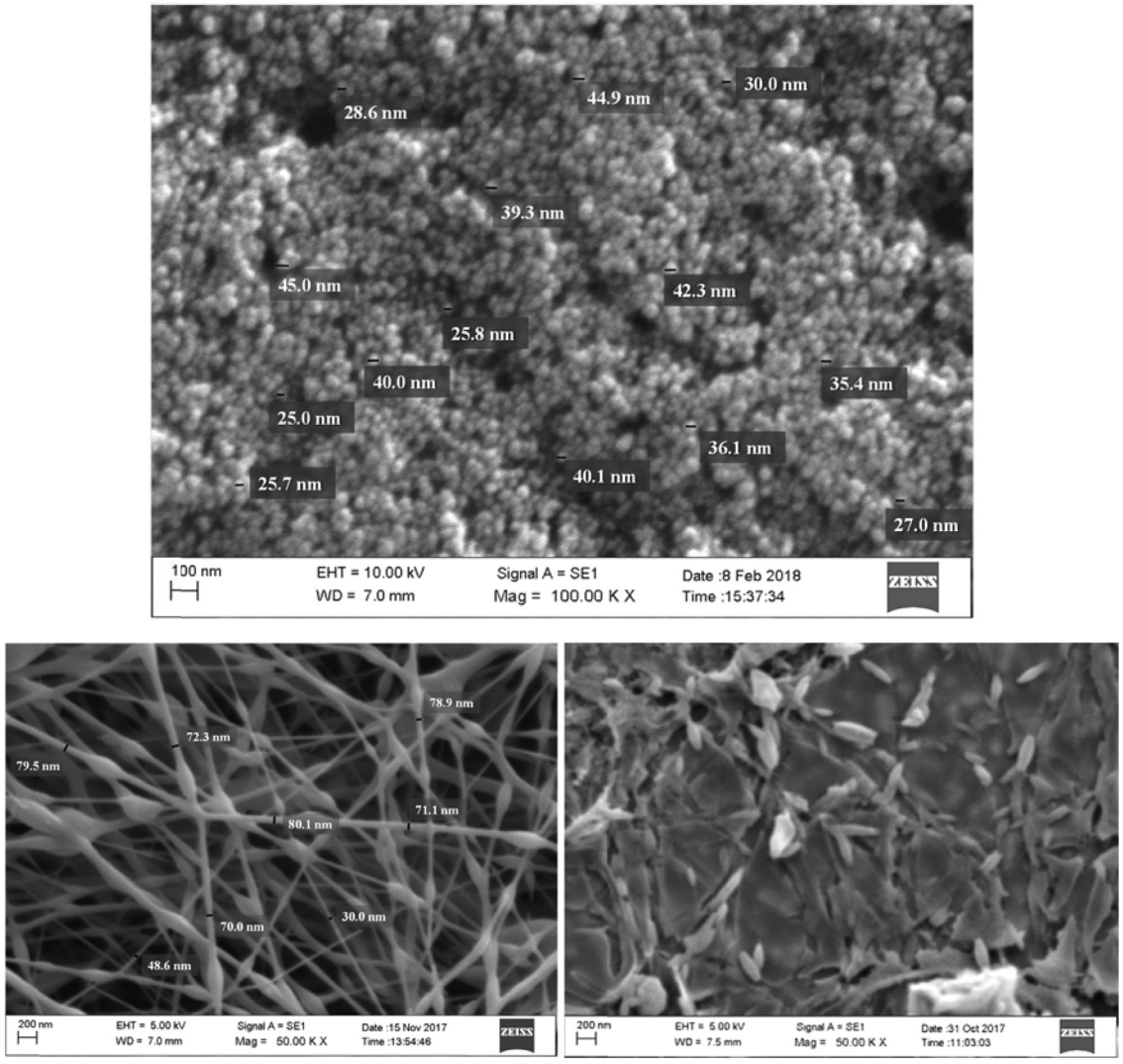

Fig. 1. (a) Top view of the first TiO_2 nanoparticle layer after sintering at 450 °C for 45 min. Particle sizes at some randomly selected places re indicated.(b) Left. Electrospun TiO_2 nanofiber layer (top view) before sintering. Diameters of fibres at some randomly selected places are indicated. Fig. 1(c) Right. Electrospun TiO_2 nanofiber layer (top view) after sintering at 450 °C for 45 min.

each QDSSC was obtained by using Autolab Potentiostat/Galvanostat PGSTAT128 N with a FRA 32 M Frequency Response Analyzer (Metrohm) under the illumination of 100 mWcm^{-2} (Solar simulator with AM 1.5 spectral filter) in the frequency interval from 0.01 Hz to 1 MHz.

3. Results and discussion

3.1. Morphology of the nanostructured photoanodes

Fig. 1(a), (b) and 1(c) show the SEM images of different TiO_2 photoanode structures used in this work. Fig. 1(a) shows the top view of the first TiO_2 P-25 nanoparticle layer spin coated on FTO/TiO_2 CL/P-90 layers after sintering. The average particle size of this nano-porous layer appears to be around 25–45 nm range. Kathirvel et al. has reported the size of the TiO_2 NP after sintering is around 35–42 nm [29]. Fig. 1(b) shows the top view of the TiO_2 nanofibre layer deposited by electrospinning on the above TiO_2 P-25 nanoparticle layer before sintering. The structure appears to consist of loosely packed, interconnected network of long nanofibres with average fibre diameter of 30–80 nm. The formation of beads can also be seen at some places. Fig. 1(c) shows the top view of the above nanofibre layer after sintering at 450 °C for 45 min. The formation of elongated, "rice grain shaped" beads non-uniformly distributed, can be seen in the structure.

It was extremely difficult to obtain a good SEM image of the cross-section view of the three layer composite photoanode structure due to the difficulty in making a delicate and sharp cut across the multilayer structure. Result from a successful attempt has been used for our analysis. Fig. 2(a) shows the cross-section SEM image of the TiO_2NP/NF/NP three-layer composite photoanode. In the cross-section image, from the bottom: Glass substrate/FTO layer/TiO_2 P-90 NP compact layer (0.67 μm)/TiO_2 P-25 NP layer (0.92 μm)/TiO_2 NF layer (0.42 μm)/TiO_2 P-25 NP layer (1.24 μm). Total thickness of the triple layer is about 2.58 μm.

Fig. 2(b) and (c) show the cross-section SEM images of the TiO_2 NP single layer and TiO_2 NP/NF double layer photoanodes. Both electrodes have the same thickness of about 2.58 μm. These are the controlled photoanodes for the triple layer structure with equal thickness.

3.2. Optical absorption of photo anodes

Fig. 3 shows the UV-VIS optical absorption spectra of TiO_2 photoanodes with equal thickness sensitized with PbS:Hg Q-dots. Each spectrum exhibits a broad absorption in the visible to near-infrared (NIR) region and a clear absorption peak can be seen at about 1050 nm. This lowest energy absorption peak is known as the "first excitonic absorption peak" of the PbS quantum dots [3]. The absorption spectrum of PbS:Hg quantum dot-loaded TiO_2 triple

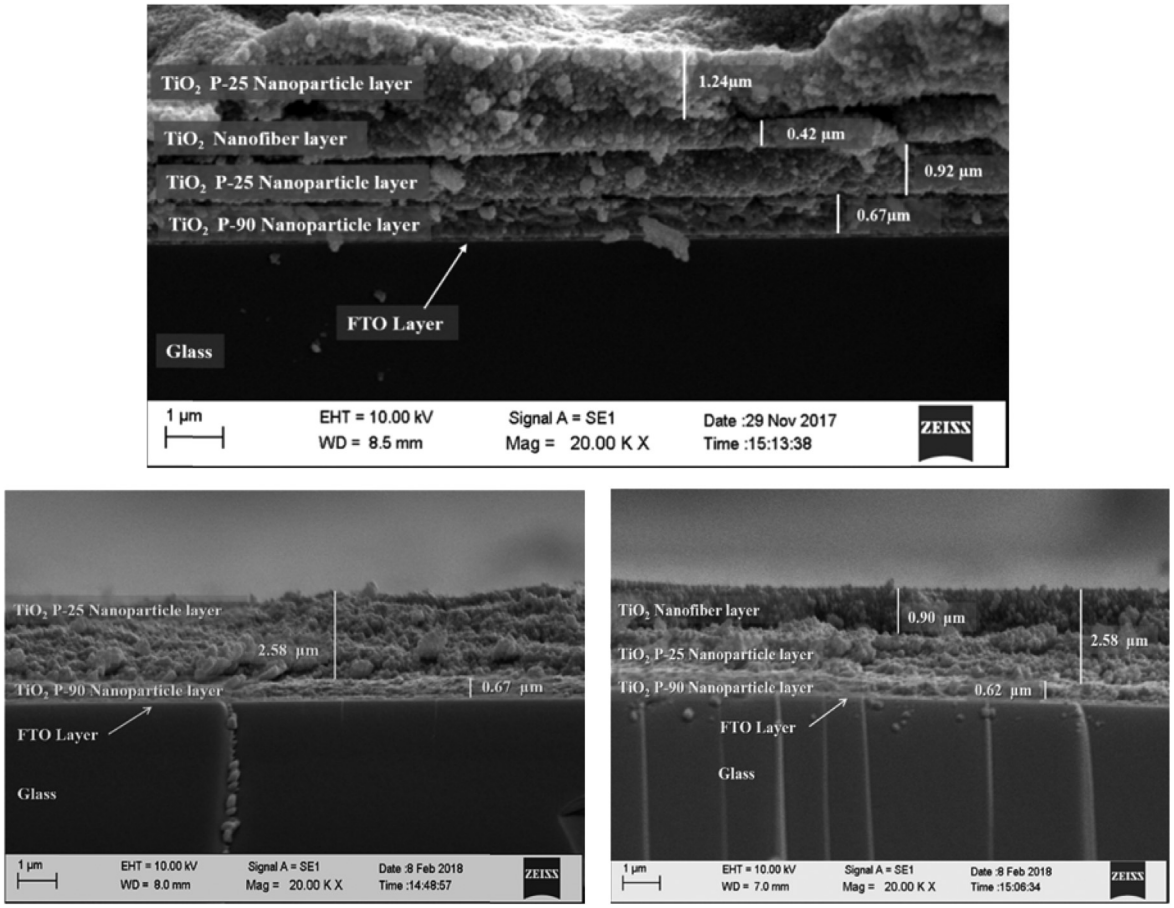

Fig. 2. (a) A cross section SEM image of the TiO_2 NP/NF/NP triple layer composite photoanode. From the bottom: Glass substrate/FTO layer/TiO_2 P-90 NP compact layer (0.67 μm)/TiO_2 P-25 NP layer (0.92 μm)/TiO_2 NF layer (0.42 μm)/TiO_2 P-25 NP layer (1.24 μm). (b) A cross section SEM image of the TiO_2 NP single layer photoanode. From the bottom: Glass substrate/FTO layer/TiO_2 P-90 NP compact layer (0.67 μm)/TiO_2 P-25 NP layer (2.58 μm); (c) A cross section SEM image of the TiO_2 NP/NF double layer photoanode. From the top: Glass substrate/FTO layer/TiO_2 P-90 NP compact layer (0.62 μm)/TiO_2 P-25 NP layer (1.68 μm)/TiO_2 NF layer (0.90 μm).

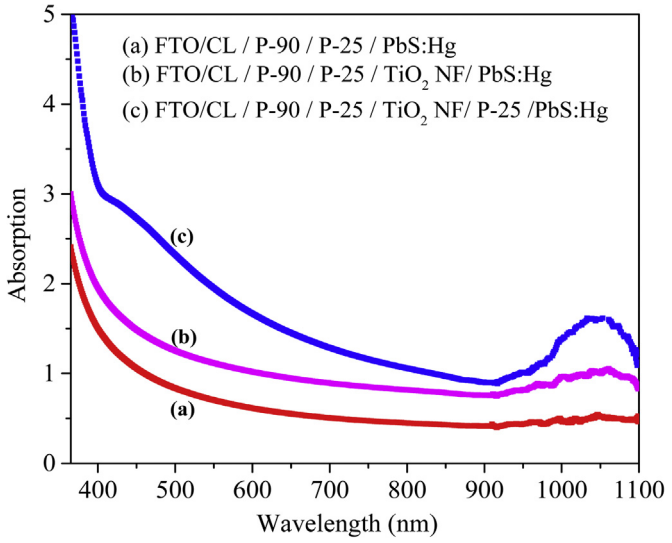

Fig. 3. Absorption spectra of PbS:Hg quantum dot-adsorbed TiO_2 photoanodes: (a) Single layer (NP), (b) Double layer (NP/NF) (c) Tri-layer(NP/NF/NP).

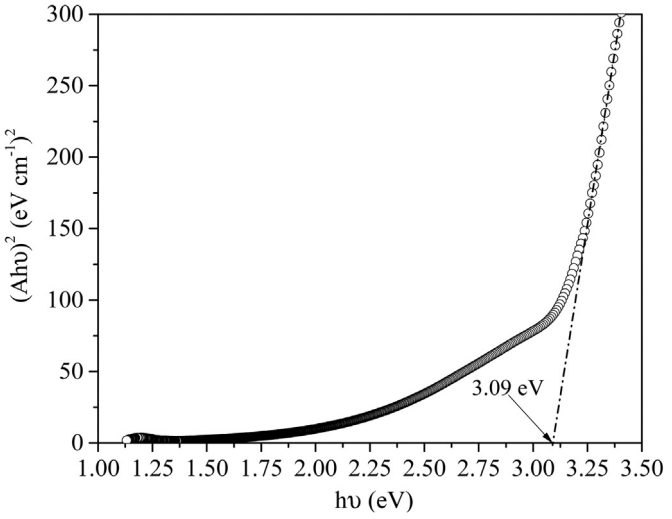

Fig. 4. $(Ah\nu)^2$ versus $(h\nu)$ plot for the determination of the optical energy transition of PbS:Hg quantum dot-sensitized TiO_2 triple layer photoanode structure.

layer structure exhibits the strongest absorption peak at 1050 nm compared to the other two photoanode structures. The TiO_2 tri-layer photoanode optimized with PbS:Hg quantum dots by SILAR cycling has undoubtedly enhanced the overall light absorption by multiple scattering effects within the nanofibre structure and by the interfaces between different TiO_2 layers. According to Fig. 3, the overall optical absorption in the visible region is enhanced by having the TiO_2 NP/NF/NP tri-layer nanostructure for the photoanode. This is evidently due to the improved light harvesting by multiple scattering effects within the tri-layer nanostructure while the PbS:Hg quantum dots appear to be responsible for the strong optical absorption in the NIR region [16,17,27]. The photon energy correspond to this wavelength is 1.18 eV and the presence of this absorption peak is consistent with visible-near IR absorption data reported by several groups on PbS colloidal Q-dots [30–33]. Sang Hyuk Im et al. have reported the presence of a strong absorption in the NIR region PbS Q-dots deposited on TiO_2 [33–35].

In the PbS:Hg Q-dot adsorbed TiO_2 photoanode nanostructure, the conduction band (CB) of bulk PbS is lower than that of TiO_2. This band positioning suppresses the injection of photogenerated electrons from PbS:Hg Q dots to the TiO_2 CB. However, this problem can be overcome by reducing the size of the PbS:Hg Q-dot particles to below the Bohr radius due to the quantum confinement. Thus, the position of the CB of the PbS:Hg Q-dots can be up-shifted by decreasing the size of Q-dots to an optimum value. Under these conditions, photo-generated electrons can be injected easily from PbS: Hg to TiO_2.

Size tunable PbS Q-dots have been synthesized by Moreels et al. [28] using $PbCl_2$ and elemental sulfur as precursors and the available size range has significantly been expanded using tri-*n*-octylphosphine (TOP) additive, enabling the synthesis of monodisperse suspensions of PbS Q-dots with a mean size varying between 3 and 10 nm. From a comparison of the peak absorption in the NIR region of our UV-VIS spectrum around 1050 nm (Fig. 3) with their published, size dependent absorption spectra, it is possible to estimate the particle size of our PbS:Hg Q-dot particles correspond to the QDSSC with highest photovoltaic performance. Accordingly, the size of our PbS:Hg Q-dots prepared using 6 SILAR cycles should be around 4.7 nm. Fig. 4 shows the plot of $(Ah\nu)^2$ versus photon energy $(h\nu)$ of the PbS:Hg Q-dot sensitized tri-layer TiO_2 photoanode which can be used to determine the energy band gap of a semiconductor material where *A* is the absorption coefficient of the material. The estimated value of the optical energy band gap of the photoanode from Fig. 4 is 3.09 eV and it appears to correspond to the shoulder around 400 nm in the UV-VIS spectra of the Q-dot sensitized, tri-layer TiO_2 photoanode (Fig. 3). This can be compared with the energy band gap of 3.4 eV pureTiO_2 nanoparticles. The shift in the optical absorption towards the longer wavelength is enhanced by the tri-layer TiO_2 photoanode structure as clearly seen from the absorption shoulder around 400 nm in Fig. 3. The effect of the Q-dot sensitization is much more pronounced with the TiO_2 NP/NF/NP tri-layer photoanode as observed by the red shift of the overall spectrum as well as by the presence of the strong absorption peak at 1050 nm in the NIR region.

3.3. Photovoltaic performance

Current density-voltage (*J-V*) measurement is the most important characterization to explore the overall photovoltaic performance of solar cells. Fig. 5 shows the photovoltaic performance of

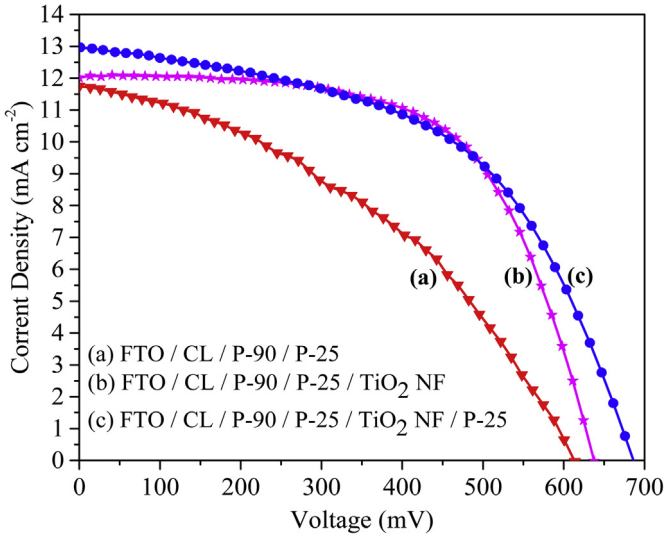

Fig. 5. Current density – voltage characterization curves of PbS:Hg QDSSCs based on different TiO_2
photoanode structures.

Table 1
Phovoltaic parameters of PbS:Hg Q-dot sensitized solar cells fabricated with (A) TiO_2 nanoparticles, (B) TiO_2 nano-particles/nano-fibres and (C) TiO_2 nano particles/nanofibers/nanoparticles.

TiO_2Photoanode	J_{SC}(mA cm^{-2})	V_{OC} (mV)	*FF* (%)	*Efficiency* (%)
A (NP)	11.78	616.1	40.56	2.94
B (NP/NF)	12.00	637.7	59.89	4.58
C (NP/NF/NP)	12.98	686.0	53.00	4.72

Table 2
EIS parameters of PbS:Hg QDSSCs with different TiO_2 photoanodes.

TiO_2 Photoanode	R_1 (Ω)	R_2 (Ω)	R_3 (Ω)
A (NP)	22.6	158.0	200.0
B (NP/NF)	21.8	143.0	412.0
C (NP/NF/NP)	20.3	128.6	419.0

the PbS:Hg Q-dot sensitized solar cells fabricated with the three types of TiO_2 photoanodes measured under 100 mW cm^{-2} (with AM 1.5 spectral filter) condition. It is clear that the TiO_2 triple layer photoanode structure based solar cell shows the best performance compared to the solar cells based on other two photoanodes. This is evidently due to the high optical absorption in the near infrared region due to the sensitization by PbS:Hg Q-dots and the enhanced optical absorption due to the multiple scattering effects in the tri-layer photoanode based solar cell. Both these factors would contribute towards efficient photogeneration of electrons and their transfer with less carrier loss.

The photovoltaic parameters of the solar cells made with the three types of TiO_2 photoandes sensitized with PbS:Hg Q-dots are summarized in Table 1. The cell with TiO_2 triple layer photoanode exhibits the highest short circuit current density and open-circuit voltage. These can be ascribed to large porous surface area and the enhanced light absorption by the tri-layer photoanode and efficient electron transport as described by Dissanayake et al. and Cuiping Kang et al. [16,17,36]. The open-circuit voltage of the triple layer TiO_2 nanostructure based solar cell shows a significant increase from 616.1 mV to 686.0 mV possibly due to the reduction of interfacial back electron transfer rate from TiO_2 to the oxidized electrolyte.

TiO_2 nanoparticle (NP)/nanofiber (NF)/nanoparticle (NP) tri-layer nanostructed photoanode has evidently improved the light harvesting by multiple scattering effects and facilitates the effective charge transport [16,17,38]. Due to the increased J_{sc} and V_{oc} values, the overall photovoltaic performance of the TiO_2 triple layer based solar cells has been significantly enhanced.

In addition to the enhancement of optical absorption by scattering in the tri-layer photoanode nanostructure, the absorption due to the high density of PbS:Hg quantum dots also enhances the photon absorption in the NIR region and increase the photocurrent of the solar cell. Triethanolamine (TEA) is a weak base which controls the surface charge of the TiO_2 nanostructure. A pH value, where a solid in a solution shows zero resultant charge on its surface is known as point of zero charge [22]. When the pH of the solution is lower than the point of zero charge, surface of the TiO_2 film is positively charged whereas when the pH is greater than the point of zero charge it is negatively charged [22,37]. In the presence of TEA, surface of TiO_2 layer becomes negative and more Pb^{2+} ions adsorb on it during the SILAR process. Due to this, the density of quantum dots is increased and the resulting photocurrent is significantly enhanced.

In this study, we fabricated Hg-doped PbS QDSSC instead of PbS QDSSC. It has already been reported that by doping with mercury, the optical absorption of the quantum dots can be red shifted [39]; this leads to enhanced light absorption and increase in the photocurrent. Annealing process of the Q-dot incorporated photoanode increases the crystallinity of PbS:Hg quantum dots and further increase the J_{SC} as described by Jianbo Gao et al. [25].

3.4. EIS analysis

Electrochemical impedance spectra of each of the solar cells made with the three types of photoanodes were analyzed by fitting the parameters with an equivalent circuit. Chemical capacitance, series resistance, charge transfer resistance and recombination resistance were determined from these data. Fig. 6 shows the Nyquist plots of the QDSSCs and the equivalent circuit model used.

CPE_1 and CPE_2 are the constant phase elements. R_1 is the series resistance which represents the FTO/TiO_2 interface, R_2 is the resistance at the counter electrode/electrolyte interface and R_3 is the resistance at the photoanode/electrolyte interface which is known as the recombination resistance. *W* is the finite Warburg

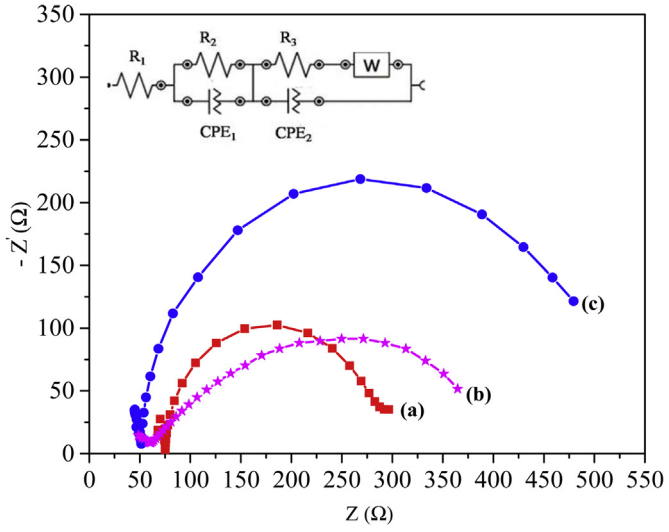

Fig. 6. Nyquist plots of PbS:Hg QDSSCs made with TiO_2 (a) single layer (b) double layer and (c) triple layer photoanode structures.

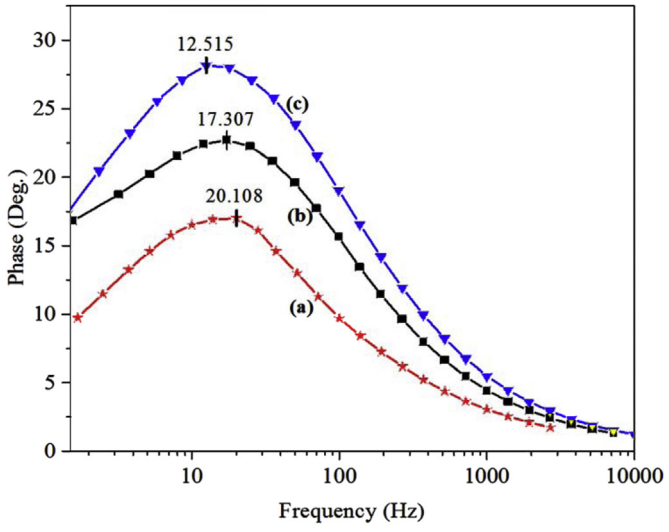

Fig. 7. Bode plots of PbS:Hg QDSSCs with TiO_2 (a) single layer (b) double layer and (c) triple layer photoanode structure.

Table 3
Comparison of electron lifetimes and photovoltaic parameters of PbS:Hg QDSSCs with different TiO_2 structures.

Photoanode	f_{max}(Hz)	τ(ms)	J_{SC}(mA cm^{-2})	Efficiency (%)
A (NP)	20.11	7.91	11.78	2.94
B (NP/NF)	17.31	9.19	12.00	4.58
C (NP/NF/NP)	12.52	12.71	12.98	4.72

impedance element which is related with diffusion process [23]. Electrochemical impedance parameters which were obtained from the circuit fitting are listed in Table 2.

TiO_2 triple layer structure shows the lowest series resistance (R_1) and the lowest charge transfer resistance (R_2) values which lead to an efficient electron transfer at the TiO_2 PbS:Hg electrode/electrolyte interface and enhance the overall performance of the cell. Also the cell with triple layer photoanode structure exhibits the highest recombination resistance (419 Ω) compared to the other two TiO_2 photoanodes. Due to this, the recombination of the electrons in the photoanode/electrolyte interface is reduced and effective electron transfer is enhanced, resulting in the increase in the J_{SC} and V_{OC} values for the cell with triple layer photoanode [40].

The Bode phase plots of the QDSSCs are shown in Fig. 7. Lifetime of the electrons can be calculated using these plots. It is clear from this figure that the frequency corresponding to the peak value for the QDSSC with TiO_2 triple layer photoanode structure has shifted to a lower value compared to QDSSCs with other two photoanodes.

Electron lifetime is inversely proportional to the peak frequency f [40] and it can be calculated from equation (1). Peak frequency values of the Bode plots and the calculated values of the electron life time for QDSSCs with three types of photoanodes are displayed in Table 3.

$$\tau = \frac{1}{2\pi f_{max}} \quad (1)$$

where, f_{max} is the frequency corresponding to the peak value.

The electrons in the TiO_2 triple layer photoanode structure have longer life times with less recombination compared to other two photoanodes suggesting that electrons are efficiently transferred resulting in a higher J_{SC} and energy conversion efficiency than the single and double layer photoanodes [23,40]. The electron lifetime (τ) is directly proportional to the recombination resistance (R_3), which is consistent with the corresponding values shown in Tables 2 and 3 as described in Jianjun Tian et al. [40].

4. Conclusion

We have synthesized PbS:Hg semiconductor quantum dots and incorporated them in Q-dot sensitized solar cells with TiO_2 based photoanodes. For the first time, we have demonstrated that the solar cells made with Q-dot sensitized tri-layer TiO_2 photoanode with configuration TiO_2 nanoparticle (NP)/nanofiber (NF)/nanoparticle (NP) exhibit significantly higher energy conversion efficiency of 4.72% compared to the cells with TiO_2 single layer (NP) and TiO_2 double layer (NP/NF). The enhanced short circuit photocurrent density and the efficiency of the tri-Layer photoanode based solar cells is evidently due to the increased light absorption covering the NIR region due to the multiple light scattering effects within the triple layer nanostructure couples with improved effective charge transport with less charge recombination. Thermal annealing effect and the increase in the number of PbS:Hg quantum dots per unit area in the TiO_2 nanostructure introduced by the weak base triethanolamine (TEA) have also contributed to the improved photovoltaic performance of these solar cells.

References

[1] A.J. Nozik, M.C. Beard, J.M. Luther, M. Law, R.J. Ellingson, J.C. Johnson, Semiconductor quantum dots and quantum qot arrays and applications of multiple exciton generation to third-generation photovoltaic solar cells, J Chem. Rev. 110 (2010) 6873.
[2] A.L. Rogach, N. Gaponik, J.M. Lupton, C. Bertoni, D.E. Gallardo, S. Dunn, N.L. Pira, M. Paderi, P. Repetto, S.G. Romanov, C. Dwyer, C.M.S. Torres, A. Eychmuller, Light-emitting diodes with semiconductor nanocrystals, Angew. Chem. Int. Ed. 47 (2008) 6538.
[3] S.A. Mcdonald, G. Konstantatosi, S. Zhang, P.W. Cyr, E.J.D. Klem, L. Levina, E.H. Sargent, Solution-processed PbS quantum dot infrared photodetectors and photovoltaics, Nat. Mater. 4 (2005) 138.
[4] S. Hoogland, V. Sukhovatkin, I. Howard, S. Cauchi, L. Levina, E.H. Sargent, A solution-processed 1.53 μm quantum dot laser with temperature-invariant emission wavelength, Optic Express 14 (8) (2006) 3273.
[5] R. Debnath, O. Bakr, E.H. Sargent, Solution-processed colloidal quantum dot photovoltaics: a perspective, J. Energy Environ. Sci. 4 (2011) 4870.
[6] J.B. Moungi, G. Bawendi, A colloidal quantum dot spectrometer, Nature 523 (2015) 67.
[7] W. Yoon, J.E. Boercker, M.P. Lumb, D. Placencia, E.E. Foos, J.G. Tischler, Enhanced open-circuit voltage of PbS nanocrystal quantum dot solar cells, Sci. Rep. 3 (2013) 2225.
[8] P. Liu, L.Y. Chen, Y.L. Lee, Effect of sodium acetate additive in successive ionic layer adsorption and reaction on the performance of CdS quantum-dot-sensitized solar cells, J. Power Sources 325 (2016) 706.
[9] V. González-Pedro, C. Sima, G. Marzari, P.P. Boix, S. Giménez, Q. Shen, T. Dittrich, I. Mora-Seró, High performance PbS quantum dot sensitized solar cells exceeding 4% efficiency: the role of metal precursors in the electron injection and charge separation, Phys. Chem. Chem. Phys. 15 (2013) 13835.
[10] A. Kongkanand, K. Tvrdy, K. Takechi, M. Kuno, P.V. Kamat, Quantum dot solar cells. Tuning photoresponse through size and shape control of CdSe–TiO_2 architecture, J. Am. Chem. Soc. 130 (2008) 4007.
[11] R.D. Schaller, V.I. Klimov, High efficiency Carrier multiplication in PbSe nanocrystals, Imp. Solar Energy Conver. 92 (2004), 186601.
[12] T.L. Li, Y.L. Lee, H. Teng, High-performance quantum dot-sensitized solar cells based on sensitization with $CuInS_2$ quantum dots/CdS heterostructure, J. Energy Environ. Sci 5 (2012) 5315.
[13] Tianxing Li, Xiaoping Zou, Hongquan, Effect of Mn Doping on properties of CdS quantum dot-sensitized solar cells, Int. J. Photoenergy 2014 (2014), 569763.
[14] J.H. Bang, P.V. Kamat, Quantum dot sensitized solar cells. A tale of two semiconductor nanocrystals: CdSe and CdTe, ACS Nano 3 (6) (2009) 1467.
[15] N. Guijarro, T. Lutz, T. Lana-Villarreal, F. O'Mahony, R. Gómez, S.A. Haque, Toward Antimony Selenide sensitized solar cells: efficient charge photogeneration at spiro-OMeTAD/Sb_2Se_3/Metal Oxide heterojunctions, J. Phys. Chem. Lett. 3 (10) (2012) 1351.
[16] M.A.K.L. Dissanayake, H.K.D.W.M.N. Divarathna, C.B. Dissanayakea, G.K.R. Senadeera, P.M.P.C. Ekanayake, C.A. Thotawattage, An innovative TiO_2 nanoparticle/nanofibre/nanoparticle, three layer composite photoanode for efficiency enhancement in dye-sensitized solar cells, J. Photochem. Photobiol. Chem. 322 (2016) 110.
[17] M.A.K.L. Dissanayake, H.N.M. Sarangika, G.K.R. Senadeera, H.K.D.W.M.N.R. Divarathna, E.M.P.C. Ekanayake, Application of a nano-structured, tri-layer TiO_2 photoanode for efficiency enhancement in quasi-solid electrolyte-based dye-sensitized solar cells, J. Appl. Electrochem. 47 (2017) 1239.
[18] F.W. Wise, Lead salt quantum dots: the limit of strong quantum confinement, Acc. Chem. Res. 33 (11) (2000) 773.
[19] A. Kiani, B.R. Sutherland, Y. Kim, O. Ouellette, L. Levina, G. Walters, C.T. Dinh, M. Liu, O. Voznyy, X. Lan, A.J. Labelle, A.H. Ip, A. Proppe, G.H. Ahmed, O.F. Mohammed, S. Hoogland, E.H. Sargent, Single-step colloidal quantum dot films for infrared solar harvesting, J. Appl. Phys. Lett. 109 (2016) 183105.
[20] L. Tao, Y. Xiong, H. Liu, W. Shen, High performance PbS quantum dot sensitized solar cells via electric field assisted in-situ chemical deposition on modulated TiO_2 nanotube array, J. Nanoscale 6 (2014) 931.
[21] M.A. Abbas, M.A. Basit, T.J. Park, J.H. Bang, Enhanced performance of PbS-sensitized solar cells via controlled successive ionic-layer adsorption and reaction, Phys. Chem. Chem. Phys. 17 (2015) 9752.
[22] J.W. Lee, J.D. Hong, N.G. Park, Six fold enhancement of photocurrent by surface charge controlled high density quantum dot coating, Chem. Commun 49 (2013) 6448.
[23] D. Punnoose, S.S. Rao, S.K. Kim, H.J. Kim, Exploring the effect of manganese in lead sulfide quantum dot sensitized solar cell to enhance the photovoltaic performance, RSC Adv. 5 (2015) 33136.
[24] P.K. Santra, P.V. Kamat, Mn-doped quantum dot sensitized solar cells: a strategy to boost efficiency over 5%, J. Am. Chem. Soc. 134 (2012) 2508.
[25] J. Gao, S. Jeong, F. Lin, P.T. Erslev, O.E. Semonin, J.M. Luther, M.C. Beard, Improvement in Carrier transport properties by mild thermal annealing of PbS quantum dot solar cells, Appl. Phys. Lett. 102 (2013), 043506.
[26] K. Meng, G. Chen, K.R. Thampi, Metal chalcogenides as counter electrode materials in quantum dot sensitized solar cells: a perspective, J. Mater. Chem. A 3 (2015) 23074.
[27] L. Li, X. Yang, J. Gao, H. Tian, J. Zhao, A. Hagfeldt, L. Sun, Highly efficient CdS

quantum dot-sensitized solar cells based on a modified polysulfide electrolyte, J. Am. Chem. Soc. 133 (2011) 8458.
[28] I. Moreels, Y. Justo, B. De Geyter, k. K.Haustraete, J.C. Martins, Z. Hens, Size-tunable, bright and stable PbS quantum dots: a surface chemistry study, ACS Nano 5 (3) (2011) 2004.
[29] Sasipriya Kathirvel, Huei-Siou Chen, Chaochin Su, Hsiue-Hsyan Wang, Chung-Yen Li, Wen-Ren Li, Preparation of smooth surface TiO2 photoanode for high energy conversion efficiency in dye-sensitized solar cells, J. Nanomaterials 2013 (2013), 367510.
[30] Zhenyu Yang, Oleksandr Voznyy, Mengxia Liu, Mingjian Yuan, Alexander H. Ip, Osman S. Ahmed, Larissa Levina, Sachin Kinge, Sjoerd Hoogland, Edward H. Sargent, ACS Nano 9 (12) (2015) 12327.
[31] C. Piliego, L. Protecescu, S.Z. Bisri, M.V. Kovalenko, M.A. Loi, 5.2% efficient PbS nanocrystal Schottky solar cells, Energy Environ. Sci. 6 (2013) 3054.
[32] Zhen Huang, Guangmei Zhai, Zhang Zhiming, Zhang Changwang, Xia Yong, Lian Linyuan, Fu Xiaoming, Zhangand Daoli, Zhang Jianbing, Low cost and large scale synthesis of PbS quantum dots with hybrid surface passivation, CrystEngComm 19 (2017) 946.
[33] Sang HyukIm, Hi-jung Kim, Sung Woo Kim, Sang-Wook Kimb, Sang Seok, All solid state multiply layered PbS colloidal quantum-dot-sensitized photovoltaic cells, Energy Environ. Sci. 4 (2011) 4181.
[34] Y.T. Ma, Y. Lin, X.R. Xiao, X.P. Li, X.W. Zhou, Synthesis of TiO_2 nanotubes film and its light scattering property, Chin. Sci. Bull. 50 (2005) 1985.
[35] S. Ito, M. Grätzel, F. Fabregat-Santiago, I. Mora-Seró, J. Bisquert, T. Bessho, H. Imai, Characteristics of high efficiency dye-sensitized solar cells, J. Phys. Chem. B 110 (2006) 25210.
[36] C. Kang, Z. Zhang, Y. Zhang, Y. He, Y. Xie, E. Xie, Enhanced efficiency in dye-sensitized solar cells using a TiO_2-based sandwiched film as photoanode, Micro Nano Lett. 6 (8) (2011) 579.
[37] M. Kosmulski, The significance of the difference in the point of zero charge between rutile and anatase, Adv. Colloid Interface Sci. 99 (2002) 255.
[38] P. Joshi, L. Zhang, D. Davoux, Z. Zhu, D. Galipeau, H. Fong, Q. Qiao, Composite of TiO_2 nanofibers and nanoparticles for dye-sensitized solar cells with significantly improved efficiency, Energy Environ. Sci. 3 (2010) 1507.
[39] R.P. Merino, O.P. Moreno, L.A. Chaltel-Lima, R.G. Pérez, M. de Icaza-Herrera, V.M. Castaño, Chemical bath deposition of PbS: Hg2+nanocrystalline thin films, J. Nanomaterials 2013 (2013), 507647.
[40] J. Tian, L. Lv, C. Fei, Y. Wang, X. Liua, G. Cao, A highly efficient (>6%) Cd1-xMnxSe quantum dot-sensitized solar cell, J. Mater. Chem. A 2 (2014) 19653.